New Journal of Physics
The open access journal at the forefront of physics

Deutsche Physikalische Gesellschaft DPG IOP Institute of Physics

PAPER • OPEN ACCESS

Superconductivity in a new layered triangular-lattice system Li_2IrSi_2

To cite this article: K Horigane *et al* 2019 *New J. Phys.* **21** 093056

New Journal of Physics
The open access journal at the forefront of physics

Deutsche Physikalische Gesellschaft DPG
IOP Institute of Physics

Published in partnership with: Deutsche Physikalische Gesellschaft and the Institute of Physics

OPEN ACCESS

RECEIVED
3 July 2019

REVISED
14 August 2019

ACCEPTED FOR PUBLICATION
4 September 2019

PUBLISHED
24 September 2019

PAPER

Superconductivity in a new layered triangular-lattice system Li_2IrSi_2

K Horigane[1], K Takeuchi[2], D Hyakumura[3], R Horie[1], T Sato[4], T Muranaka[5], K Kawashima[3], H Ishii[6], Y Kubozono[1], S Orimo[4,7], M Isobe[8] and J Akimitsu[1]

[1] Research Institute for Interdisciplinary Science, Okayama University, Okayama, Japan
[2] Graduate School of natural science and technology, Okayama University, Okayama, Japan
[3] Department of Physics and Mathematics, Aoyama Gakuin University, Sagamihara, Japan
[4] Institute for Materials Research, Tohoku University, Sendai, Japan
[5] Department of Engineering Science, University of Electro-Communications, Tokyo, Japan
[6] National Synchrotron Radiation Research Center, Hsinchu, Taiwan
[7] WPI-Advanced Institute for Materials Research (AIMR), Tohoku University, Sendai, Japan
[8] National Institute for Materials Science (NIMS), Tsukuba, Japan

Keywords: supreconductivity, iridium-silicide, spin–orbit coupling

Abstract

We report on the crystal structure and superconducting properties of a novel iridium-silicide, namely Li_2IrSi_2. It has a Ag_2NiO_2-type structure (space group R-3m) with the lattice parameters $a = 4.028\,30(6)$ Å and $c = 13.161\,80(15)$ Å. The crystal structure comprises $IrSi_2$ and double Li layers stacked alternately along the c-axis. The $IrSi_2$ layer includes a two-dimensional Ir equilateral-triangular lattice. Electrical resistivity and static magnetic measurements revealed that Li_2IrSi_2 is a type-II superconductor with critical temperature (T_c) of 3.3 K. We estimated the following superconducting parameters: lower critical field $H_{c1}(0) \sim 42$ Oe, upper critical field $H_{c2}(0) \sim 1.7$ kOe, penetration depth $\lambda_0 \sim 265$ nm, coherence length $\xi_0 \sim 44$ nm, and Ginzburg–Landau parameter $\kappa_{GL} \sim 6.02$. The specific-heat data suggested that superconductivity in Li_2IrSi_2 could be attributed to weak-coupling Cooper pairs.

1. Introduction

Owing to their unique physical properties, including charge and spin ordering, colossal magnetoresistance, and high-T_c superconductivity, 3*d* transition-metal compounds have attracted considerable attention. These physical properties emerge from the interplay between spin, charge, and orbital degrees of freedom. On the contrary, 5*d* transition-metal compounds are expected to exhibit exotic phenomena, because their spin–orbit coupling (SOC) is significantly stronger than that of 3*d* transition-metal compounds. The non-centrosymmetric superconductivity discovered in $CePt_3Si$ [1] and UIr [2] is a typical example of effective physical property enhancement by SOC, wherein Cooper pairs develop a spontaneous magnetic moment below the superconducting transition temperature (T_c), breaking the time-reversal symmetry. The superconducting wave function is described as a mixed-parity state of spin-singlet and triplet Cooper pairs. Another typical case is the spin–orbit Mott state in Sr_2IrO_4 proposed by Kim *et al*, wherein an effective total angular moment $j_{eff} = 1/2$ Kramers doublet state is produced by an on-site Coulomb repulsion U associated with strong SOC in a 5*d* electron system [3]. Watanabe *et al* theoretically predicted that the electron-doped SO Mott state would exhibit *d*-wave superconductivity due to the pseudospin of the $j_{eff} = 1/2$ Kramers doublet [4]. In recent angle-resolved photoemission spectroscopy experiments, *d*-wave symmetry in the superconducting gap order parameter was observed in electron-doped Sr_2IrO_4 [5]. Therefore, 5*d* electron systems, particularly in Ir compounds, involve rich physics, which are interesting research subjects for the exploration of novel exotic superconductivity.

Several Ir-based superconductors have been reported till date, which include MIr_2As_2 (M = Sr, Ba, Y, La) [6–9], $Ir_{1-x}Pt_xTe_2$ [10–12], $SrIr_2$ [13], B_2IrT_2 (T = Mo, V) [14], ThIr, MIr_2 (M = Sc, Y, La), MIr_3 (M = La, Th, Ce), MIr_5 (M = La, Th, Ce), Y_3Ir_2 [15], IrGe [16], $M_5Ir_4Si_{10}$ (M = Sc, Y, Lu), $M_5Ir_4Ge_{10}$ (M = Y, Lu) [17–20], $IrTe_3$ [21], MIr_2Si_2 (M = Y, La) [22], and Li_2IrSi_3 [23, 24]. Among these superconductors, $Sc_5Ir_4Si_{10}$ has the highest T_c of ~8.5 K, which is ascribed to the large density of states (DOS) at the Fermi level (E_F) with moderate

electron–phonon coupling [25]. In general, Si often reacts with 4d- or 5d-elements (M) to form a variety of silicide intermetallics because the energy levels of the Si 3p and M 4d or 5d orbitals are close together, resulting in orbital hybridization and unfilled metallic bands near E_F. Orbital hybridization generates M-Si covalent bonding network in the structure. In $Sc_5Ir_4Si_{10}$, a $Co_4Sc_5Si_{10}$-type structure, the three-dimensional network comprised an Ir–Si cyclic octagonal lattice. A two-dimensional (2D) network is formed by Ir–Si tetrahedral linkage in $LaIr_2Si_2$, a $ThCr_2Si_2$-type structure. A metallic state with a large DOS at E_F is expected in iridium silicides. This would be advantageous for the development of new superconductors because large electron densities can lead to Cooper pairing coherency. In fact, several Ir–Si superconductors, such as $Sc_5Ir_4Si_{10}$ ($T_c \sim 8.5$ K), $Lu_2Ir_3Si_5$ ($T_c \sim 5.6$ K), $CaIrSi_3$ ($T_c \sim 3.6$ K), and HfIrSi ($T_c \sim 3.5$ K), have been reported [26–29]. These superconductors comprised primarily of rare-earth or alkali-earth compounds. To the best of our knowledge, Li_2IrSi_3 ($T_c = \sim 3.8$ K) is the only alkali-metal compound reported till date. Therefore, the alkali-metal Ir–Si ternary system is an unexplored subject in new materials research, which motivated us to perform this study.

After numerous attempts to synthesize new alkali-metal iridium silicides, we recently produced a new superconductor, Li_2IrSi_2, using a high-pressure synthesis technique. Li_2IrSi_2 has a layered structure composed of planar equilateral triangular Ir lattices and it exhibits a superconducting transition at ~3.3 K. Therefore, Li_2IrSi_2 is a rare superconductor with a 2D Ir triangular lattice. Its crystal structure, a triangular Ir lattice, is similar to that of $IrTe_2$. However, in contrast to $Ir_{1-x}Pt_xTe_2$ ($T_c = \sim 3.1$ K), superconductivity in Li_2IrSi_2 occurs at low temperatures without breaking chemical bonds [10]. Herein, we report the crystal structure and superconducting properties of Li_2IrSi_2 and present its superconducting parameters estimated from experimental critical field measurements. We also comment briefly on another new superconductor, Li_2RhSi_2, which is isostructural to Li_2IrSi_2. Furthermore, we discuss the relation between the SOC and superconductivity in this material.

2. Experimental procedures

Polycrystalline samples of Li_2IrSi_2 were prepared using a solid-state reaction with a high-pressure synthesis technique. Commercial chemicals, Ir (4N) and Si (4N) powders, and handmade precursor ($Li_{12}Si_7$) were used as starting materials. The precursor $Li_{12}Si_7$ was prepared from a stoichiometric mixture of Li lumps and Si powder in a solid-sate reaction at 800 °C for 30 min, which was post-annealed at 450°C for 16 h in an evacuated quartz tube. The starting materials were mixed in an agate mortar at a molar ratio of Li:Ir:Si = 2:1:2 and then pressed into a disk shape with a diameter and thickness of 6.9 and ~3.5 mm, respectively. The chemicals in these procedures were handled in a glove box filled with dry argon gas. The pellets were put in a high-pressure cell with a pressure medium of hexagonal boron nitride (h-BN) powder. Then, they were reacted at 1250 °C for 15 min under 3 GPa using a flat-belt-type high-pressure apparatus installed at the National Institute for Materials Science (NIMS) in Japan, followed by quenching to room temperature before pressure release [30].

Powder x-ray diffraction (XRD) data were collected at room temperature using a conventional diffractometer (Rigaku; RINT-TTR III) with Bragg-Brentano geometry and a Cu-K_α radiation source. The collected Bragg peak positions were analyzed using the TREOR97 indexing program [31]. Synchrotron powder XRD experiments were conducted using a diffractometer equipped with Debye–Scherrer geometry and curved-surface imaging-plate detector installed at the SPring-8 BL12B2 beamline. The incident beam, with a wavelength (λ) = 0.6857 Å, was focused in a 250 μm^2 size using a toroidal mirror. A capillary with a diameter of 0.5 mm was used for a powder-sample holder. The synchrotron XRD data were analyzed using the Rietveld method with the software RIETAN2000 [32].

Magnetic measurements were performed using a superconducting quantum interference device magnetometer (Quantum Design, MPMS-R2). The magnetic data were collected for a pulverized sample encapsulated by nonmagnetic material. Electrical resistivity was measured with the standard DC four-probe method using a commercial apparatus (Quantum Design, PPMS). The excitation current was set to either 1.0 or 5.0 mA. The data were collected at temperatures between 1.9 and 200 K under various magnetic fields up to 2 kOe. Specific heat was measured with the PPMS according to the time-relaxation method. The data were collected with a small bulk specimen at temperatures between 2 and 10 K under magnetic fields of 0 and 90 kOe.

3. Results and discussion

3.1. Crystal structure

Figure 1(a) shows the powder XRD patterns. The top pattern (red) is that of Li_2IrSi_2 sample. The middle (blue) pattern was a calculated based on the Li_2IrSi_2 phase with the structural model shown in figure 2(a) (*v.i.*). The bottom (green) pattern is that of the known phase, Li_2IrSi_3 [23, 24]. The observed Li_2IrSi_2 pattern (top) could be reproduced from the calculated pattern (middle), and they were undoubtedly different from that of Li_2IrSi_3. The

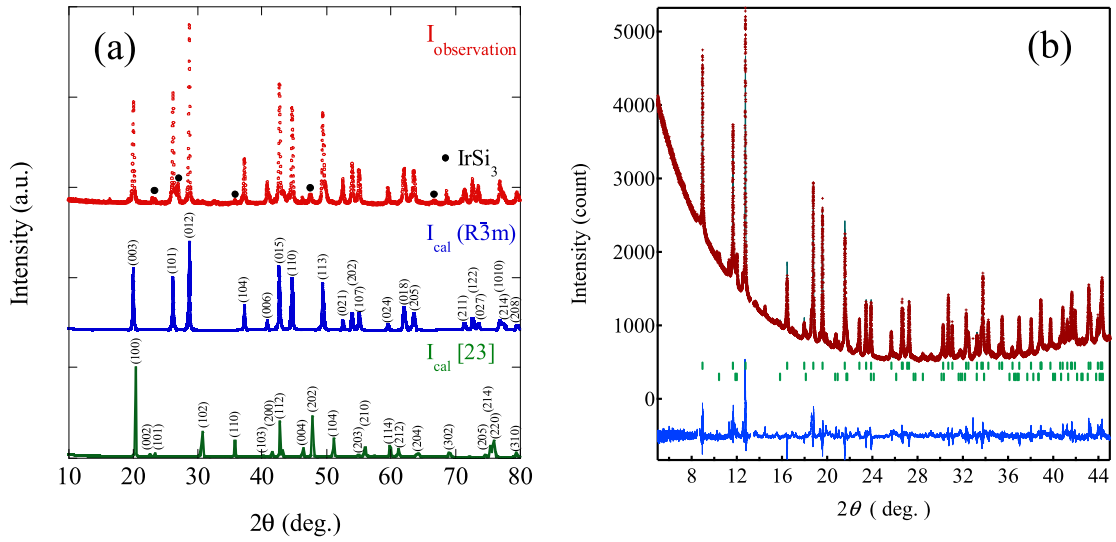

Figure 1 (a) Powder x-ray diffraction (XRD) patterns of Li_2IrSi_2. The observed pattern is shown at the top (red circles). The middle pattern (blue line) was calculated with the structural model shown if figure 2(a). The bottom pattern (green line) is an XRD pattern of Li_2IrSi_3 [23]. (b) Synchrotron XRD pattern of Li2IrSi2 and the Rietveld-analysis profile with the structural model in figure 2(a).

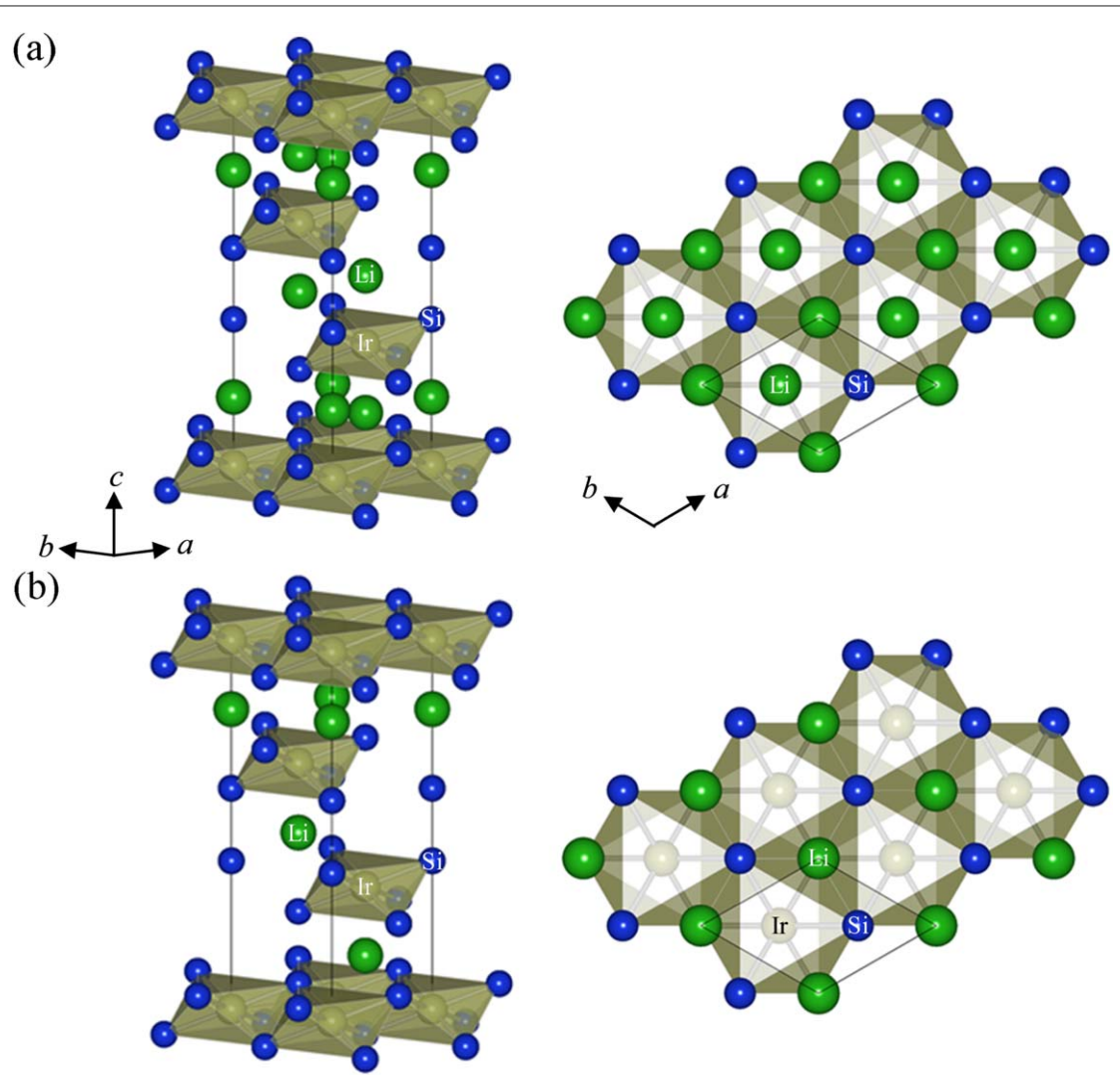

Figure 2. Crystal structure models of (a) Li_2IrSi_2 (space group R-3m) and (b) $LiIrSi_2$ (*R*3m). The former includes Li bilayers placed at the octahedral position, while the latter includes Li monolayers placed at the prismatic position.

Table 1. Crystal structure parameters of Li_2IrSi_2.

Atom	Site	Occupancy	x	y	z
Li	6c	1	0	0	0.1875(6)
Ir	3a	1	0	0	0
Si	6c	1	0	0	0.5982(1)
Formula	Li_2IrSi_2				
Molecular weight	262.27				
Space group	R3m (no. 166)				
Lattice constants	$a = 4.028\ 30(5)$ Å, $c = 13.161\ 80(15)$ Å, $V = 184.9650(44)$ Å^3				
Z	3				
Density (calculated)	7.063 654 g cm^{-3}				
Temperature	Room temperature				
Wave length	0.685 671 Å				
R factor	$R_{wp} = 3.72\%$, $R_P = 2.46\%$, $S = R_{wp}/Re = 1.2559$				
Refinement software	RIETAN-2000				

XRD pattern observed for the Li_2IrSi_2 sample indicates a new phase, which is not in the PDXL (Rigaku) database. Majority of the Bragg reflections can be indexed to a trigonal unit cell with lattice parameters a and c as $\sim$ 4.03 and $c \sim 13.16$ Å, respectively. The extinctions are $-h + k + l = 3n$ for hkl and $l = 3n$ for $00l$ reflections, where n is an integer. Therefore, the potential space groups are centrosymmetric R-3m (No. 166) and R-3 (148) and non-centrosymmetric R32 (155), R3m (160), and R3 (146). Li_2IrSi_2 has rhombohedral symmetry. The sample also contains a small amount of a secondary phase, non-superconducting $IrSi_3$.

Herein, we propose a crystal structure model for Li_2IrSi_2 with the space group R-3m, which is the group with the highest symmetry of those mentioned above, as shown in figure 2(a). This is the Ag_2NiO_2-type structure. The structure model comprised closed-packed stacking of equilateral-triangle lattice planes of Ir, Si, and Li atoms with rhombohedral symmetry. The atomic layer sequence in a period along the c-axis is …Ir, Si)-(Li, Li)-(Si, Ir, Si)-(Li, Li)-(Si, Ir, Si)-(Li, Li)-(Si, Ir… for the closed-packed positions …a, b)-(c, a)-(b, c, a)-(b, c)-(a, b, c)-(a, b)-(c, a …, respectively. The structure includes $IrSi_2$ layers interleaved with a Li bilayer, stacked alternately along the c-axis. The $IrSi_2$ layer comprises edge-shared $IrSi_6$ octahedrons. The Li atom has octahedral (six-fold) coordination with the adjacent atoms.

Based on the structural model in figure 2(a), the atomic coordinates were refined by Rietveld analysis of the synchrotron XRD data. Figure 1(b) shows the synchrotron XRD pattern. A multiphase pattern-fitting method was used for the analysis of the primary (Li_2IrSi_2) and secondary ($IrSi_3$) phases. The resultant reliability factors were $R_{wp} = 3.72\%$, $R_P = 2.46\%$, and $S = R_{wp}/R_e = 1.2559$, which were satisfactorily low. The mass fraction of the secondary phase ($IrSi_3$) included in the sample was estimated to be ~9.3%. We also performed Rietveld refinement of the Li site occupancy, and we could refine ~10% of the Li vacancies in the structure. However, our refinement could not determine the thermal factor B (we fixed $B = 1$) which is strongly correlated with the occupancy of atom and the reliability factor of this defect model was nearly identical to that of the non-defect model. The chemical formula thus needs to be confirmed with another method, such as energy dispersive x-ray spectroscopy. For this reason, we do not address Li vacancy quantitatively in this report. The refined structural parameters for Li_2IrSi_2 are listed in table 1.

We tested the other space groups R-3, R32, R3m, and R3 to describe the Ag_2NiO_2-type structural model. These space groups have a lower symmetry than R-3m. Since the space groups R-3 and R32 give the same structural model as R-3m, these space groups can be excluded from the candidates. The non-centrosymmetric space groups R3m and R3 give a structural model similar to that of R-3m. They give additional structural parameters describing the asymmetry of the atomic position. However, it was found that these space groups did not effectively lower the reliability factors. Therefore, it is unlikely that the space groups R3m and R3 actually describe the structure.

Furthermore, we tested other possible cases of the structural model, which were relates to Li defects in the structure because Li is a volatile and light element and is insensitive to detection by XRD measurements. If the structure contains heavy Li defects, the Li atomic layer may be a monolayer rather than a bilayer. In this case, the atomic layer sequence would be …Ir, Si)-(Li)-(Si, Ir, Si)-(Li)-(Si, Ir, Si)-(Li)-(Si, Ir…, therefore, the molecular formula is actually $LiIrSi_2$. Figure 2(b) illustrates a structural model for the $CuCrSe_2$-$NaVS_2$-type structure (space group R3m), where Li has a prismatic (six-fold) coordination with adjacent Si atoms. We analyzed the XRD data with this structural model and found that it gave a rather similar XRD pattern to the observed one. However, it was less satisfactory for reliability factors than the Ag_2NiO_2-type structure. Therefore, it seemed unlikely that the $CuCrSe_2$-$NaVS_2$-type structural model fully described the actual structure. For $LiIrSi_2$, another

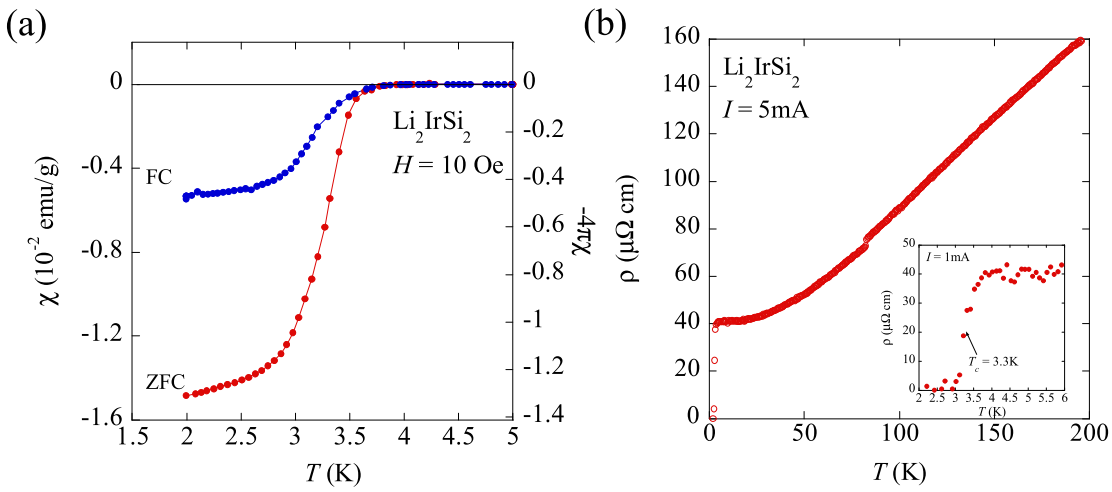

Figure 3 (a) Temperature (T) dependence of the magnetic susceptibility (χ) of Li_2IrSi_2. (b) Temperature dependence of the electrical resistivity (ρ) of Li_2IrSi_2. A magnification of the resistivity data in the low-temperature region is shown in the inset.

possible structural model was delafossite-type $NaCrS_2$ (R-3m), which had a different stacking manner for the $IrSi_2$ layer block than the $CuCrSe_2$-$NaVS_2$ type. We confirmed that the XRD pattern calculated with this structural model was essentially different from the observed pattern. Therefore, delafossite-type $NaCrS_2$ apparently did not represent $LiIrSi_2$.

Resultantly, we concluded that the structural model with the Ag_2NiO_2 type (space group R-3m) in figure 2(a) was the most suitable for the crystal structure in Li_2IrSi_2. Li_2IrSi_2 with quasi-2D layer structure, including Ir equilateral-triangular lattice planes. This structure strongly contrasted with the quasi-1D columnar structure of Li_2IrSi_3 [23, 24]. The Ir–Si bond lengths in Li_2IrSi_2 (2.495 Å) and Li_2IrSi_3 (2.463 Å) were nearly the same. The atomic compositions of the compounds were similar; however, their structures were essentially different.

3.2. Superconducting properties

Superconductivity in Li_2IrSi_2 was observed in magnetic and electrical resistivity measurements. Figure 3(a) shows the temperature (T) dependence of the magnetic susceptibility (χ) taken under a magnetic field (H) of 10 Oe. Diamagnetic Meissner signals were observed below 3.6 K ($\sim T_c^{onset}$). The magnitude of the superconducting signal at 2 K was ~47% of the full Meissner volume fraction ($-1/4\pi$) for the field-cooling (FC) condition and ~131% for zero-field-cooling (ZFC). The signal was sufficiently large to indicate that superconductivity was a natural property of the bulk material. The value in excess of 100% suggested that the observed signal was affected by demagnetization and magnetic penetration under the magnetic field.

Figure 3 (b) shows the T-dependence of the electrical resistivity (ρ) of Li_2IrSi_2. The T-dependence between 4 and 50 K in the normal state followed the T-square law, $\rho = \rho_0 + AT^2$, suggesting Fermi-liquid behavior. The inset in figure 3 shows the low-temperature resistivity data. At ~3.6 K, the resistivity started to drop due to the superconducting transition. The observed critical temperature, $T_c^{onset} = 3.6$ K, was consistent with that of the magnetic susceptibility measurements. The bulk T_c defined as the midpoint of resistive transition was 3.3 K.

Figure 4 (a) shows initial magnetization (M–H) curves measured at various temperatures below T_c^{onset} (=3.6 K), which exhibited type-II superconductor behavior. The lower critical field $H_{c1}(T)$ at each temperature was defined as the magnetic field at which the magnetization began to deviate from the straight line tangent to the curve at $H = 0$ in figure 4(a). The H_{c1} values are plotted as a function of temperature in figure 4(c). Based on the Ginzburg–Landau (GL) theory, the $H_{c1}(T)$ curve was numerically fitted using the following equation:

$$H_{c1}(T) = H_{c1}(0)\left\{1 - \left(\frac{T}{T_c}\right)^2\right\}, \quad (1)$$

where $H_{c1}(0) = 42$ Oe. Figure 4(b) shows the T-dependence of the electrical resistivity below 5 K under various magnetic fields. The onset and midpoint T_c values are plotted as a function of the magnetic field in figure 4(d). $H_{c2}(T)$ monotonically increased with decreasing temperature. The upper critical fields $H_{c2}(0)$ determined from the linear extrapolation of the observed onset and midpoint T_c data were estimated to be ~2.6 and 1.28 kOe, respectively. To determine H_{c2} more precisely, we measured the specific-heat in this system.

Figure 5 shows the specific-heat data for Li_2IrSi_2, specifically C_p/T versus T^2 plots measured at $H = 0$ and 90 kOe. At $H = 0$, a specific-heat jump was observed around ~3.5 K, indicating that the superconductivity is a bulk property. The phase-transition temperature is consistent with the T_c values determined from the electrical

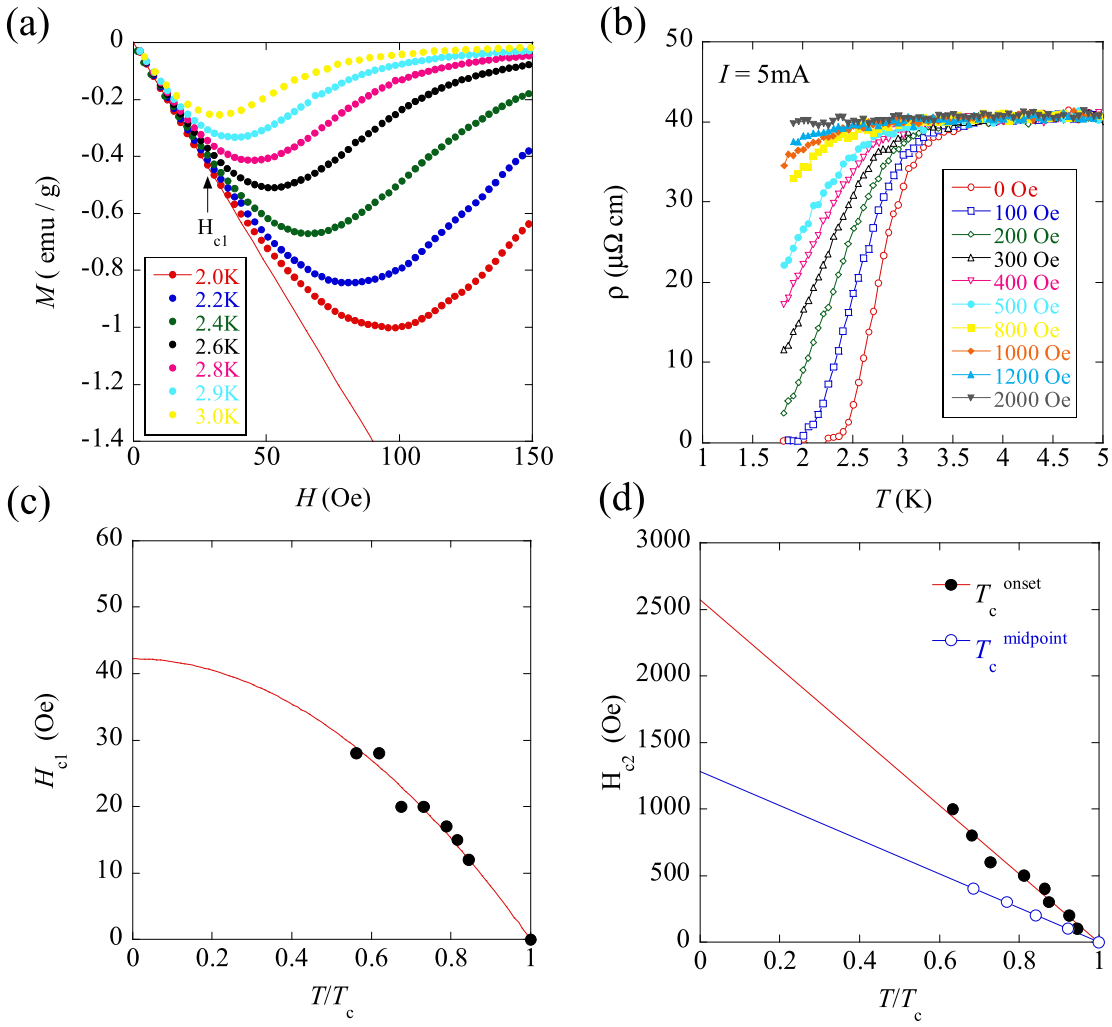

Figure 4 (a) Initial magnetization curve (M–H curve) of the superconducting state in Li_2IrSi_2 measured at temperatures below T_c^{onset} (=3.6 K). (b) Temperature dependence of electrical resistivity (ρ) for the superconducting transition of Li_2IrSi_2, measured under the various magnetic fields. (c) Lower critical field H_{c1} plotted as a function of normalized temperature (T/T_c). The solid curve indicates numerical fitting of the data points with equation (1) (see text). (d) The upper critical field H_{c2} plotted as a function of normalized temperature (T/T_c). The solid red and blue lines represent linear extrapolation to $T = 0$ K and give $H_{c2}(0) \sim 2.6$ kOe (T_c^{onset}) and 1.28 kOe ($T_c^{midpoint}$), respectively.

resistivity and the magnetic susceptibility measurements. At $H = 90$ kOe, the specific-heat jump disappeared completely. The normal-state specific heat (at $H = 90$ kOe) can be given by

$$\frac{C_p}{T} = \gamma_N + \beta T^2, \tag{2}$$

where γ_N is the Sommerfeld constant of the normal state, and β is the specific-heat coefficient of the lattice part. The Debye temperature can be written as $\Theta_D = (12\pi^4 NR/5\beta)^{1/3}$, where N is the number of atoms in a formula unit and R is the gas constant. By numerically fitting the dataset in equation (2), the initial values, γ_{N0} and β_0, were first determined. Since γ_{N0} and β_0 include the contribution from the secondary phase $IrSi_3$, we corrected the values by subtracting the impurity contribution to estimate intrinsic γ_N and β for Li_2IrSi_2. Herein, we used the parameters reported in [24] for $IrSi_3$, $\gamma_N' \sim 0.73$ mJ mol^{-1} K^{-2} and $\beta \sim 0.057$ mJ mol^{-1} K^{-4}, with a mass fraction of $IrSi_3$ (~9.3%) in the sample. The resultant parameters intrinsic to Li_2IrSi_2 are $\gamma_N = 4.16$ mJ mol^{-1} K^2 and $\beta = 0.1868$ mJ mol^{-1} K^4, i.e. $\Theta_D = 373$ K.

The thermal critical field $H_c(0)$ was estimated by $0.236\gamma_N T_c^2 = \mu_0 H_c(0)^2/2$. The thermodynamic critical field $H_c(0)$ was ~0.27 kOe; therefore, the value of $H_{c2}(0)$ subsequently calculated by $H_c(0)^2 = H_{c1}(0) \times H_{c2}(0)$ was 1.7 kOe. The estimated superconducting coherence length ξ_0 was ~44 nm. This is based on $H_{c2}(0) = \Phi_0/2\pi\xi_0^2$, where Φ_0 is the fluxoid quantum (=2.0678 $\times$ 10^{-7} Gcm^2). The London penetration depth λ_0 and GL parameter κ_{GL} were determined to be ~265 nm and ~6.02, respectively. These were obtained the GL equation, $H_{c1}(0) = [\Phi_0/4\pi\lambda_0^2] \times \ln(\kappa_{GL})$, where $\kappa_{GL} = \lambda_0/\xi_0$. The κ_{GL} value (>1) indicates that Li_2IrSi_2 is a type-II superconductor. The superconducting parameters are listed in table 2.

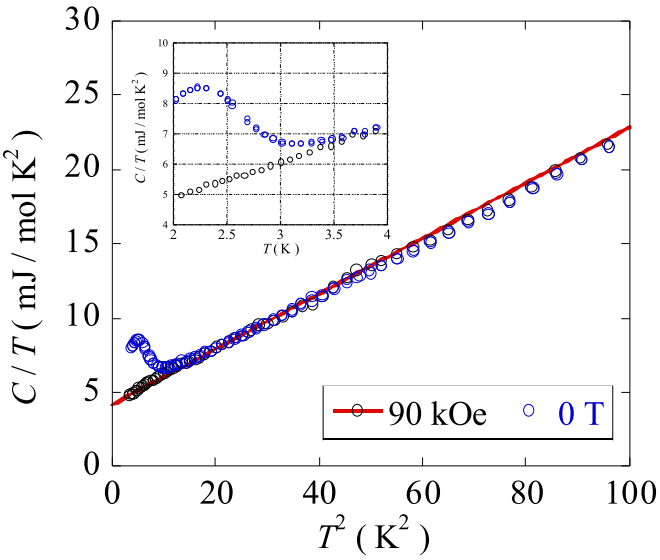

Figure 5 Specific-heat data (C_p/T versus T^2 plots) for Li_2IrSi_2 collected at 0 and 90 kOe. The solid straight line indicates numerical fitting of the data points with equation (2) (see text), which gives the Sommerfeld constant (γ_N, ~4.2 mJ mol^{-1} K^2) and the Debye temperature (Θ_D, ~370 K). An enlargement of the plots around T_c^{onset} (=3.5 K) is shown in the inset.

Table 2. Superconducting parameters and physical properties in Li_2IrSi_2.

	Li_2IrSi_2
T_c(K)	3.3
$H_{c1}(0)$ (Oe)	42
$H_{c2}(0)$ (kOe)	1.7
$H_c(0)$ (kOe)	0.27
$\lambda(0)$ (nm)	265
$\xi(0)$ (nm)	44
κ_{GL}	6.02
γ_N (mJ mol^{-1} K^{-2})	4.16
β (mJ mol^{-1} K^{-4})	0.1868
Θ (K)	373
$N(\varepsilon_F)$ (states/eV/f.u.)	1.76

Assuming that the conventional phonon-mediated Cooper pairing mechanism is realized in Li_2IrSi_2, we evaluated the strength of the electron–phonon coupling. According to McMillan's theory [33], the electron–phonon coupling constant λ_{ep} is written as follows:

$$\lambda_{ep} = \frac{1.04 + \mu^* \ln\left(\frac{\Theta_D}{1.45T_c}\right)}{(1 - 0.62\mu^*)\ln\left(\frac{\Theta_D}{1.45T_c}\right) - 1.04}, \quad (3)$$

where μ^* is the Coulomb pseudo-potential parameter. By substituting the experimental Θ_D value (~373 K) and standard value of $\mu^* = 0.1$ into equation (3), we estimated $\lambda_{ep} \sim 0.5$, which suggests that Li_2IrSi_2 is a weak-coupling superconductor. The electronic DOS at the Fermi level $N(E_F)$ can be given by as follows:

$$N(E_F) = \frac{3\gamma_N}{\pi^2 k_B^2 (1 + \lambda_{ep})}. \quad (4)$$

For Li_2IrSi_2, by substituting the obtained γ_N and λ_{ep} values into equation (4), $N(E_F)$ was estimated to be ~1.2 states/eV/f.u. This value is close to the DOS value ($N(E_F) \sim 1.1$ states/cell/f.u.) of the Ir–Si superconductor $BaIrSi_2$ ($T_c \sim 6$ K) [34].

We are curious how the SOC affects the superconducting properties. From this viewpoint, it is interesting to clarify the relation between the SOC and superconductivity by substituting Rh for Ir in Li_2IrSi_2. In general, Rh (4d element) provides more moderate SOC than Ir (5d element). Recently, we succeeded in synthesizing a new

rhodium silicide superconductor Li_2RhSi_2 that is isostructural to Li_2IrSi_2. Its critical temperature T_c^{onset} is ~3.0 K, which is a little lower than the T_c^{onset} (~3.6 K) of Li_2IrSi_2. It is important to clarify whether or not the difference between the T_c values is due to the difference in the SOC of Rh and Ir. Therefore, it is necessary to precisely evaluate the superconducting parameters and gap structure in Li_2RhSi_2, which is the focus of further studies that are now in progress.

4. Summary

We successfully discovered a new Ir–Si superconductor, Li_2IrSi_2, with $T_c = 3.3$ K. The crystal structure is a rhombohedral system with the lattice constants *a* and *c* of 4.028 30(6) and 13.161 80(15) Å, respectively. We have proposed a structural model with space group R-3m (figure 2 (a)), which comprises edge-shared $IrSi_2$ layers interleaved with a Li bilayer. The $IrSi_2$ layer includes a quasi-2D Ir equilateral triangular lattice as an electron conduction plane. Superconductivity in Li_2IrSi_2 is type-II and is a bulk property. The superconducting parameters are as follows: lower critical field $H_{c1}(0) \sim 42$ Oe, upper critical field $H_{c2}(0) \sim 1.7$ kOe, penetration depth $\lambda_0 \sim 265$ nm, coherence length $\xi_0 \sim 44$ nm, Ginzburg–Landau parameter $\kappa_{GL} \sim 6.02$, and electron–phonon coupling constant $\lambda_{ep} \sim 0.5$. It seems that Li_2IrSi_2 is a conventional weak-coupling superconductor. The influence of SOC on its superconductivity is still unclear.

Acknowledgments

This work was supported by Grants-in-Aid from the Ministry of Education, Culture, Sports, Science and Technology (MEXT) under Grants No. 2704, and was partially supported by NIMS Joint Research Hub Program, Research Subsidy from Electric Power Development Co., Ltd (Dengenkaihatsu), and Program for Advancing Strategic International Networks to Accelerate the Circulation of Talented Researchers from Japan Society for the Promotion of Science (R2705).

ORCID iDs

K Horigane https://orcid.org/0000-0003-3338-9115
Y Kubozono https://orcid.org/0000-0002-7910-0308

References

[1] Bauer E, Hilscher G, Michor H, Paul C, Scheidt E W, Gribanov A, Seropegin Y, Noël H, Sigrist M and Rogl P 2004 *Phys. Rev. Lett.* **92** 027003
[2] Akazawa T, Hidaka H, Fujiwara T, Kobayashi T C, Yamamoto E, Haga Y, Settai R and Onuki Y 2004 *J. Phys. Condens. Matter* **16** L29
[3] Kim B J *et al* 2008 *Phys. Rev. Lett.* **101** 076402
[4] Watanabe H, Shirakawa T and Yunoki S 2013 *Phys. Rev. Lett.* **110** 027002
[5] Kim Y K, Sung N H, Denlinger J D and Kim B J 2016 *Nat. Phys.* **12** 37
[6] Wang X C, Ruan B B, Yu J, Pan B J, Mu Q G, Liu T, Chen G F and Ren Z A 2017 *Supercond. Sci. Technol.* **30** 035007
[7] Hirai D, Takayama T, Hashizume D, Higashinaka R, Yamamoto A, Hiroko A K and Takagi H 2010 *Physica* C **470** S296
[8] Braun H F, Engel N and Parthé E. 1983 *Phys. Rev.* B **28** 1389
[9] Hirjak M, Lejay P, Chevalier B, Etourneau J and Hagenmuller P 1985 *J. Less-Common Met.* **105** 139
[10] Pyon S, Kudo K and Nohara M 2012 *J. Phys. Soc. Japan* **81** 053701
[11] Ootsuki D *et al* 2014 *J. Phys. Soc. Japan* **83** 033704
[12] Ootsuki D *et al* 2012 *Phys. Rev.* B **86** 014519
[13] Matthias B T and Corenzwit E 1957 *Phys. Rev.* **107** 1558
[14] Vandenberg J M, Matthias B T, Corenzwit E and Barz H 1975 *Mat. Res. Bull.* **10** 889
[15] Geballe T H, Matthias B T, Compton V B, Corenzwit E, Hull G W and Longinotti L D 1965 *Phys. Rev.* **137** A119
[16] Matthias B T 1953 *Phys. Rev.* **92** 874
[17] Sun Y, Ding Y, Gu D, Zhuang J, Shi Z and Tamegai T 2013 *J. Phys. Soc. Japan* **82** 074713
[18] Yang H D, Shelton R N and Braun H F 1986 *Phys. Rev.* B **33** 5062
[19] Shelton R N, Hausermann-Berg L S, Klavins P, Yang H D, Anderson M S and Swenson C A 1986 *Phys. Rev.* B **34** 4590
[20] Hausermann-Berg L S and Shelton R N 1987 *Phys. Rev.* B **35** 6659
[21] Raub C J, Compton V B, Geballe T H, Matthias B T, Maita J P and Hull G W 1965 *J. Phys. Chem. Solids* **26** 2051
[22] Vališka M, Pospíšil J, Prokleška J, Diviš M, Rudajevová A and Sechovský V 2012 *J. Phys. Soc. Japan* **81** 104715
[23] Hirai D, Kawakami R, Magdysyuk O V, Dinnebier R E, Yaresko A and Takagi H 2014 *J. Phys. Soc. Japan* **83** 103703
[24] Pyon S *et al* 2014 *J. Phys. Soc. Japan* **83** 093706
[25] Lue C S, Liu R F, Fu Y F, Cheng C and Yang H D 2008 *Phys. Rev.* B **77** 115130
[26] Singh Y, Pal D, Ramakrishnan S, Awasthi A M and Malik S K 2005 *Phys. Rev.* B **71** 045109
[27] Eguchi G, Wadati H, Sugiyama T, Ikenaga E, Yonezawa S and Maeno Y 2012 *Phys. Rev.* B **86** 184510
[28] Xian-Zhong W, Chevalier B, Etourneau J and Hagenmuller P 1985 *Mat. Res. Bull.* **20** 517
[29] NIMS Material Database (*Mat Navi*) https://mits.nims.go.jp/index_en.html

[30] Isobe M, Yoshida H, Kimoto K, Arai M and Takayama-Muromachi E 2014 *Chem. Mater.* **26** 2155
[31] Werner P-E, Eriksson L and Westdahl M 1985 *J. Appl. Crystallogr.* **18** 367
[32] Izumi F and Ikeda T 2000 *Mater. Sci. Forum* **321–324** 198
[33] McMillan W L 1968 *Phys. Rev.* **167** 331
[34] Isobe M, Kimoto K, Arai M and Takayama-Muromachi E 2019 *Phys. Rev.* B **99** 054514